Evidence for Microbial Carbon and Sulfur Cycling in Deeply Buried Ridge Flank Basalt

Mark A. Lever *et al.*

Science **339**, 1305 (2013);
DOI: 10.1126/science.1229240

Science (print ISSN 0036-8075; online ISSN 1095-9203) is published weekly, except the last week in December, by the American Association for the Advancement of Science, 1200 New York Avenue NW, Washington, DC 20005.

The difference in XAS and participator decay positions of the 2π* state can be related to nuclear dynamics during the core hole lifetime in XES (*24*). The smaller spectator shift in XES, lower participator intensity of the excited 2π* electron, and less shifted 2π* XAS resonance show that the CO molecules that have broken the direct CO metal bond have not yet desorbed into gas phase but still interact weakly with the surface.

Using DFT, we examined (figs. S9 and S10) the 1s→2π* core-excited states and spectra for different points along the minimum energy path of Fig. 3. The computed XAS spectra reproduce the expected behavior with enhanced 2π* intensity together with a shift to higher energy as the distance to the surface increases. In the precursor state, the antibonding CO orbitals, which have a large spatial extent, still interact with the metal states. The substrate interaction with the 2π* has a distance dependence in the precursor state, and most likely, we are probing a distribution of distances in the experiment; rotation of the molecule in the precursor potential has only minor effects on the spectra (fig. S10).

Because 30% of the $\tilde{d}_\pi$ intensity disappeared and the spectra could be fitted with 30% shifted gas-phase contributions at long delay times, it is likely that 30% of the molecules were pumped into the precursor state, supporting the notion that the two states have rather comparable free energies. Some of the molecules desorb during the experiment, but when the system cools, the remaining molecules can return from the precursor to the chemisorbed state. Previous SFG results showed that the C-O stretch intensity was reduced by one order of magnitude after a pump laser pulse that led to a final desorption of ~30% of the adsorbed CO molecules (*8*, *12*). However, the SFG intensity recovered to half of its initial value after 170 ps (*8*) because roughly half of the molecules readsorbed into the chemisorbed state. We suggest that the initial drop of intensity in the SFG experiment corresponds to essentially all of the molecules being pumped into the precursor state, in which the SFG signal would disappear because of orientational disordering of the CO molecules (*25*, *26*). Because the laser fluence in the SFG experiment and in the present experiment are similar, we propose that also in the present case, ~50% of the molecules return to the chemisorbed state from the precursor state as the substrate cools down and the temperature-induced entropic barrier to the chemisorbed state vanishes. The molecules in the precursor state have very weak interactions perpendicular to the surface, which leads to a small probability of obtaining the perpendicular momentum needed for desorption. Considering, on the other hand, the time-reversed situation, a similar trapping in the precursor state due to the entropic barrier must also occur in chemisorption.

The prefactors in Arrhenius expressions for desorption rates of molecules such as CO are often anomalously large (*27*). For instance, the prefactor for CO desorption on Ru(0001) has been found to be of the order 10^{14} to 10^{19} s^{-1}, depending on coverage (*21*), versus typical values between 10^{12} and 10^{13} s^{-1}; this has generally been explained by the difference in entropy between the initial (adsorbed) state and the final (gas) state (*21*). We instead found that it is the entropy gain at the free-energy barrier between the chemisorbed and precursor state that is decisive. In the present case, this leads to a computed prefactor on the order of 10^{17} s^{-1} and, consequently, to the efficient population of the precursor state observed in our experiment.

References and Notes

1. A. Cassuto, D. A. King, *Surf. Sci.* **102**, 388 (1981).
2. D. J. Doren, J. C. Tully, *Langmuir* **4**, 256 (1988).
3. P. Kisliuk, *J. Phys. Chem. Solids* **3**, 95 (1957).
4. J. B. Taylor, I. Langmuir, *Phys. Rev.* **44**, 423 (1933).
5. C. Frischkorn, M. Wolf, *Chem. Rev.* **106**, 4207 (2006).
6. H. Arnolds, M. Bonn, *Surf. Sci. Rep.* **65**, 45 (2010).
7. E. H. G. Backus, A. Eichler, A. W. Kleyn, M. Bonn, *Science* **310**, 1790 (2005).
8. M. Bonn *et al*., *Phys. Rev. Lett.* **84**, 4653 (2000).
9. F. Fournier, W. Zheng, S. Carrez, H. Dubost, B. Bourguignon, *J. Chem. Phys.* **121**, 4839 (2004).
10. I. M. Lane, D. A. King, Z. P. Liu, H. Arnolds, *Phys. Rev. Lett.* **97**, 186105 (2006).
11. K. Inoue, K. Watanabe, Y. Matsumoto, *J. Chem. Phys.* **137**, 024704 (2012).
12. Materials and methods, and supporting analysis of the experimental and theoretical data, are available as supplementary materials on *Science* Online
13. A. Föhlisch, W. Wurth, M. Stichler, C. Keller, A. Nilsson, *J. Chem. Phys.* **121**, 4848 (2004).
14. A. Nilsson, L. G. M. Pettersson, *Surf. Sci. Rep.* **55**, 49 (2004).
15. A. Nilsson *et al*., *Phys. Rev. Lett.* **78**, 2847 (1997).
16. A. Föhlisch *et al*., *J. Chem. Phys.* **112**, 1946 (2000).
17. O. Björneholm *et al*., *Phys. Rev. B* **46**, 10353 (1992).
18. L. Bartels, F. Wang, D. Möller, E. Knoesel, T. F. Heinz, *Science* **305**, 648 (2004).
19. J. Wellendorff *et al*., *Phys. Rev. B* **85**, 235149 (2012).
20. M. Dion, H. Rydberg, E. Schröder, D. C. Langreth, B. I. Lundqvist, *Phys. Rev. Lett.* **92**, 246401 (2004).
21. H. Pfnür, P. Feulner, D. Menzel, *J. Chem. Phys.* **79**, 4613 (1983).
22. D. J. Doren, J. C. Tully, *J. Chem. Phys.* **94**, 8428 (1991).
23. C. Keller *et al*., *Phys. Rev. Lett.* **80**, 1774 (1998).
24. P. Skytt *et al*., *Phys. Rev. A* **55**, 134 (1997).
25. Y. R. Shen, *Principles of Non-Linear Optics* (Wiley-Interscience, New York, 2003)
26. J. H. Hunt, P. Guyot-Sionnest, Y. R. Shen, *Chem. Phys. Lett.* **133**, 189 (1987).
27. I. Chorkendorf, H. Niemantsverdriet, *Concepts of Modern Catalysis and Kinetics* (Wiley-VCH, Weinheim, Germany, 2003).

Acknowledgments: This work is supported by the U.S. Department of Energy (DOE), Office of Basic Energy Sciences, Division of Materials Sciences and Engineering, under contract DE-AC02-76SF00515; the DOE, Basic Energy Science through the SUNCAT Center for Interface Science and Catalysis; the Swedish National Research Council; the Danish Center for Scientific Computing; the Volkswagen Stiftung; the Alexander von Humboldt Foundation; and the Lundbeck Foundation. The spectrum calculations were performed on resources provided by the Swedish National Infrastructure for Computing (SNIC) at the High Performance Computing Center North. Portions of this research were carried out on the SXR Instrument at LCLS, a division of SLAC National Accelerator Laboratory and an Office of Science user facility operated by Stanford University for the DOE. The SXR Instrument is funded by a consortium whose membership includes the LCLS, Stanford University through SIMES, Lawrence Berkeley National Laboratory, University of Hamburg through the BMBF priority program FSP 301, and the Center for Free Electron Laser Science.

Supplementary Materials

www.sciencemag.org/cgi/content/full/339/6125/1302/DC1
Materials and Methods
Figs. S1 to S12
References (*28*–*50*)

18 October 2012; accepted 27 December 2012
10.1126/science.1231711

Evidence for Microbial Carbon and Sulfur Cycling in Deeply Buried Ridge Flank Basalt

Mark A. Lever,[1,2]* Olivier Rouxel,[3,4] Jeffrey C. Alt,[5] Nobumichi Shimizu,[3] Shuhei Ono,[6] Rosalind M. Coggon,[7] Wayne C. Shanks III,[8] Laura Lapham,[2]† Marcus Elvert,[9] Xavier Prieto-Mollar,[9] Kai-Uwe Hinrichs,[9] Fumio Inagaki,[10] Andreas Teske[1]*

Sediment-covered basalt on the flanks of mid-ocean ridges constitutes most of Earth's oceanic crust, but the composition and metabolic function of its microbial ecosystem are largely unknown. By drilling into 3.5-million-year-old subseafloor basalt, we demonstrated the presence of methane- and sulfur-cycling microbes on the eastern flank of the Juan de Fuca Ridge. Depth horizons with functional genes indicative of methane-cycling and sulfate-reducing microorganisms are enriched in solid-phase sulfur and total organic carbon, host $\delta^{13}C$- and $\delta^{34}S$-isotopic values with a biological imprint, and show clear signs of microbial activity when incubated in the laboratory. Downcore changes in carbon and sulfur cycling show discrete geochemical intervals with chemoautotrophic $\delta^{13}C$ signatures locally attenuated by heterotrophic metabolism.

Subseafloor basaltic crust represents the largest habitable zone by volume on Earth (*1*). Chemical reactions of basalt with seawater flowing through fractures release energy that may support chemosynthetic communities. Microbes exploiting these reactions are known

from basalt exposed at the seafloor, where the oxidation of reduced sulfur (S) and iron (Fe) from basalt with dissolved oxygen and nitrate from seawater supports high microbial biomass and diversity (*2*, *3*). Multiple lines of indirect evidence that include textural alterations (*4*), depletions in δ^{34}S-pyrite (FeS_2) (*5*) and δ^{13}C-dissolved inorganic carbon (DIC) (*6*), and DNA sequences from borehole observatories (*7*, *8*) suggest active microbial communities in subseafloor basalt.

We combined sequencing of genes diagnostic of microbial methane and S cycling with geochemical and isotopic analyses of C and S pools and laboratory-based incubations to directly identify microbial ecosystem components in deep subseafloor basalt. The 3.5-million-year-old basement at site U1301 was sampled during Integrated Ocean Drilling Program (IODP) Expedition 301 in 2004 (fig. S1) (*9*). Site U1301, off the eastern flank of the Juan de Fuca Ridge, is covered by a 265-m-thick sediment layer and lies ~2 km south of ODP Site 1026, which it resembles in temperature profile, lithology, and sediment chemistry (*9*). Given anticipated poor recovery due to brecciation of the upper basement [265 to 350 m below seafloor (mbsf)], coring was restricted to an interval of pillow basalts and massive lavas (351 to 583 mbsf). Sulfate concentrations (~16 mM) and vein carbonates indicate that basalt fluids are derived from seawater, which enters ~55 km south at Grizzly Bare outcrop and discharges near U1301, at Baby Bare and Mama Bare outcrops (*9*, *10*) (fig. S1B). Yet, the basement at U1301 differs from seafloor-exposed basalt in its uniformly high temperature (~64°C) (*9*) and lack of fresh photosynthesis-derived organic matter, dissolved oxygen, and nitrate (*7*, *11*). These conditions preclude oxygen- or nitrate-dependent microbial S and Fe oxidation (*12*) but may enable growth of anaerobes, such as sulfate reducers and methanogens, which use sulfate and DIC as electron acceptors.

We sequenced genes encoding the α subunit of methyl coenzyme M reductase (*mcrA*), a gene unique to methanogens and anaerobic methane oxidizers (*13*), and the β subunit of dissimilatory sulfite reductase (*dsrB*), a gene found in sulfate- and sulfite-reducing microbes (*14*), to indicate the presence of methane-cycling

[1]Department of Marine Sciences, University of North Carolina at Chapel Hill, Chapel Hill, NC 27599, USA. [2]Center for Geomicrobiology, Department of BioScience, Aarhus University, DK-8000 Aarhus C, Denmark. [3]Woods Hole Oceanographic Institution, Woods Hole, MA 02543, USA. [4]IFREMER, Centre de Brest, 29280 Plouzané, France. [5]Department of Earth and Environmental Sciences, University of Michigan, Ann Arbor, MI 48109, USA. [6]Department of Earth, Atmospheric, and Planetary Sciences, Massachusetts Institute of Technology, Cambridge, MA 02139, USA. [7]Department of Earth Science and Engineering, Imperial College London, South Kensington Campus, London SW7 2AZ, UK. [8]U.S. Geological Survey, Denver, CO 80225, USA. [9]Organic Geochemistry Group, Department of Geosciences and MARUM Center for Marine Environmental Sciences, University of Bremen, D-28334 Bremen, Germany. [10]Geomicrobiology Group, Kochi Institute for Core Sample Research, Japan Agency for Marine-Earth Science and Technology, Nankoku, Kochi 783-8502, Japan.

*To whom correspondence should be addressed. E-mail: mark.lever@biology.au.dk (M.A.L.); teske@email.unc.edu (A.T.)

†Present address: University of Maryland Center for Environmental Science, Solomons, MD 20688, USA.

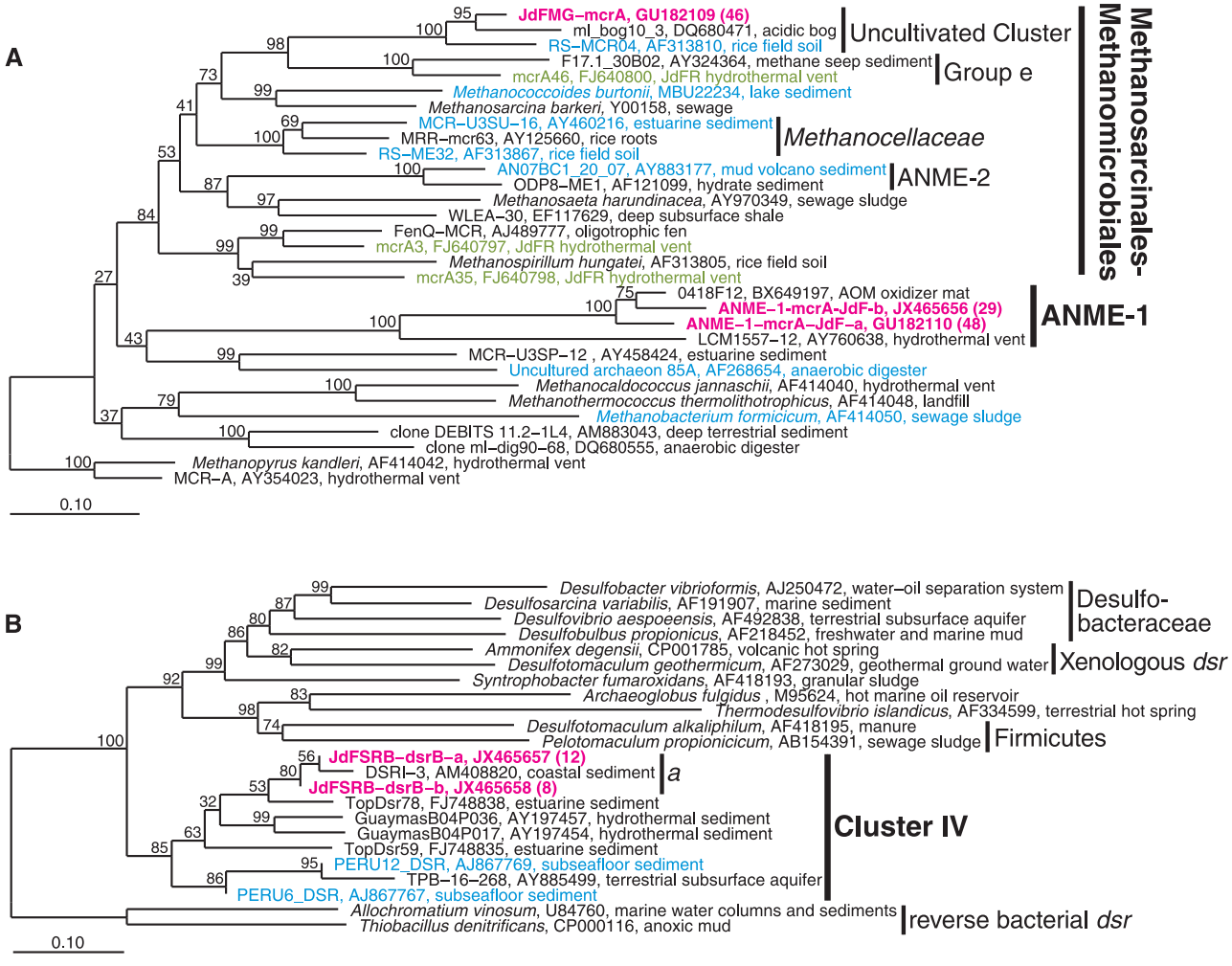

Fig. 1. Phylogenetic trees of functional genes. (**A**) *McrA* sequences from borehole U1301B are in bold magenta. Close relatives based on microarray analyses of JdF Ridge hydrothermal vent chimneys and seafloor basalt are in green (*18*) and cyan (*19*), respectively. (**B**) *DsrB* sequences from borehole U1301B are in bold magenta and sequences from subseafloor sediment off Peru in cyan (*22*). Bootstrap support (in %, 1000 replications) is indicated at each branching point.

and sulfate-reducing microbes. We detect *mcrA* in 5 of the 10 samples and *dsrB* in 4 of the 6 samples tested (table S1), which suggests that these metabolisms are present in this environment.

The phylogenetic diversity of *mcrA* genes that we identified is restricted to two groups: the Juan de Fuca Methanogen Group (JdFMG), which falls into an uncultivated cluster within the *Methanosarcinales*, and anaerobic methane-oxidizing archaea (ANME-1) (Fig. 1A). Close relatives of the JdFMG have been identified from paddy and wetland soil (*15*, *16*) and also have been found in marine habitats, including Juan de Fuca Ridge hydrothermal vent chimneys and seafloor-exposed basalt ~100 km west of U1301 (fig. S2) (*17*, *18*). ANME-1 occur widely in marine sediments and methane seeps and are believed to gain energy from the anaerobic oxidation of methane (AOM) (*19*). Two distinct ANME phylotypes occur at U1301, one closely related to ANME-1 from methane seeps and another clustering with only one other sequence, from subseafloor sediment (fig. S3). We detected JdFMG in 4 and ANME-1 in 3 out of 10 basalt samples. Two samples contained both groups (table S1).

The phylogenetic diversity of *dsrB* in these samples is limited to one group, the Juan de Fuca Sulfate Reducing Group (JdFSRG), which falls into Cluster IV, a deeply branching *dsrB* cluster without cultured members, first reported from hydrothermal sediment (Fig. 1B, fig. S4, and table S1) (*20*). Remarkably, the only other *dsr* sequences reported so far from the subseafloor—in sediment of the Peru Margin (*21*)—also fall into this cluster, which is widespread in shallow marine sediment and terrestrial aquifers.

We studied solid-phase S pools by analyzing acid-volatile sulfide (AVS), chromium-reducible S (CRS), and sulfate-S (SO_4-S) as a proxy to redox processes and correlate to microbial metabolisms (*5*, *22*). We found *dsrB* sequences only in a relatively reduced "intermediate depth interval" (~430 to 520 mbsf, samples 14R to 26R) in samples with AVS as the main S pool in alteration halos (14R-1-11)—the visually conspicuous zone surrounding fractures (fig. S1C)—or in host rock (17R-170, 20R-1-57, and 23R-2-21) (fig. S5 and table S1). Samples from this interval have higher AVS, CRS, and total S (fig. S5 and table S2); contain large pyrite fronts (14R-1-65P, 15R-4-142P) (fig. S5); and have lower δ^{34}S-AVS, -CRS, and -SO_4-S, compared with the more oxidized upper (1R to 12R) and lower coring intervals (30R to 36R) (fig. S6 and table S1). Consistent with higher Fe^{3+}/Fe^{Total} ratios, which indicate halos to be more oxidized than host rock (table S1), pyrite is generally absent from halos or veins. Outside the intermediate depth interval, the near absence of pyrite from host rock, and mixed clay-Fe-oxyhydroxide–dominated halos and veins, are further evidence of pervasive oxidative alteration.

We analyzed the δ^{34}S signature of pyrite grains to examine micro- and macroscale variations in microbial S cycling (tables S1 and S3 and Fig. 2). Although variable, the δ^{34}S-pyrite grains [–72.4 to 1.2 per mil (‰)] (table S3) are typically lower than those of AVS (–9.3 to –0.2‰),

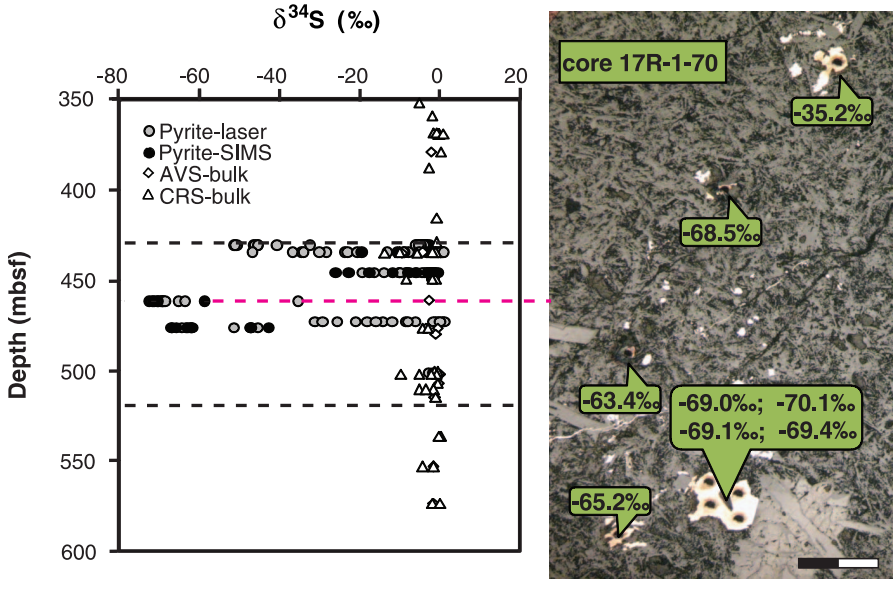

Fig. 2. Macro- and microscale distribution of S-isotopic data. On the left, δ^{34}S-depth profile of pyrite granules, analyzed by laser ablation and secondary ion mass spectrometry (SIMS), and bulk S pools (AVS and CRS). On the right, thin-section micrograph showing individual pyrite granules and their δ^{34}S. The dashed magenta line indicates the sampling depth of the thin section. The dashed black lines mark the intermediate depth interval. Pyrite grains with a sufficient diameter for δ^{34}S determination (10 μm) were limited to this interval. Scale bar, 200 μm.

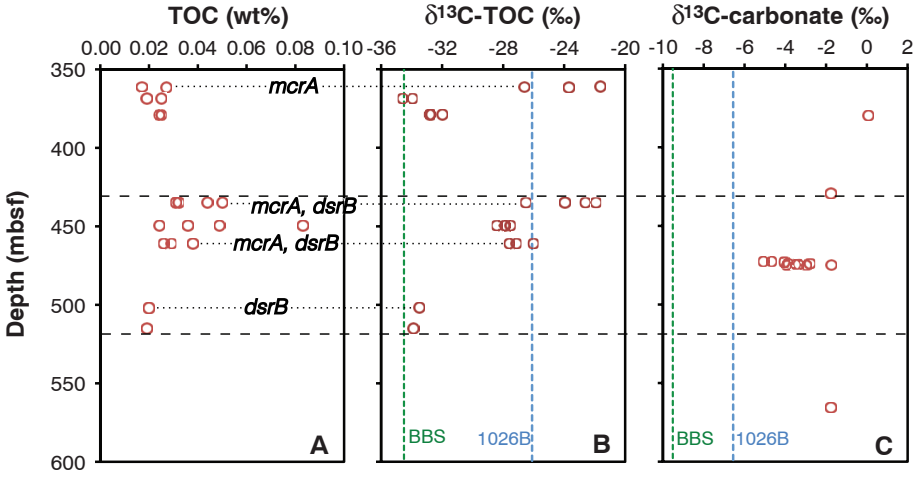

Fig. 3. Depth-related trends in (**A**) TOC content, (**B**) δ^{13}C-TOC, and (**C**) δ^{13}C-carbonate. Cores with functional gene detection are indicated in (A) and (B). Dashed vertical lines indicate δ^{13}C-DOC (B) and δ^{13}C-DIC (C) values from 1026B and BBS. Because the carbonate content of rock samples used in (A) and (B) was too low for analyses, δ^{13}C from carbonate veins are shown in (C). The reduced intermediate depth interval falls between the dashed horizontal lines. All δ^{13}C are in ‰ versus Vienna Pee Dee belemnite (VPDB).

CRS (–13.7 to 0‰), SO_4-S (–6.5 to 0‰), mantle S (0‰) (*5*), dissolved sulfate in bottom sediments at ODP Site 1026 (+30‰) (*23*), or seawater (+21‰) (Fig. 2). Locally, the $\delta^{34}S$ of pyrite grains reach very negative values (–72‰), consistent with the addition of highly ^{34}S-depleted secondary sulfide to basement rock (*22*). These low $\delta^{34}S$-pyrite values indicate single-step sulfate reduction (*24*) or repeated cycles of sulfate reduction and S oxidation (*25*). The co-occurrence of low $\delta^{34}S$-pyrite, *dsrB*, and *mcrA* of ANME-1 in two samples (14R-1-11, 17R-1-70) suggests local coupling between methane and S cycling by sulfate-dependent AOM.

Depth profiles of total organic carbon (TOC) content, $\delta^{13}C$-TOC, and $\delta^{13}C$-carbonate at U1301B are consistent with functional gene and ^{34}S data (Fig. 3). The TOC content is highest in the intermediate depth interval in cores with *mcrA*, *dsrB*, and low $\delta^{34}S$-pyrite (Fig. 3A and table S4). The $\delta^{13}C$-TOC is in the range of dissolved organic C (DOC) in fluids from nearby 1026B and Baby Bare Springs (BBS) (Fig. 3B and table S4) and lower than seawater DOC (–21.1‰) (*6*). The $\delta^{13}C$-carbonate is higher than $\delta^{13}C$-DIC at Site 1026B or BBS (Fig. 3C and table S5) and overlaps with $\delta^{13}C$-DIC of bottom seawater (–1.4‰) (*10*).

$\delta^{13}C$-TOC values in the upper coring interval (4R to 5R) and near the bottom (23R to 26R; –34.6 to –32.0‰) are close to $\delta^{13}C$-DOC from nearby BBS (–34.6‰) (Fig. 3B). The absence of O_2 and the high ^{13}C-TOC depletion relative to carbonate (~–30 to –35‰) suggest C fixation by the reductive acetyl CoA pathway—an anaerobic pathway found in all methanogens and acetogens and certain sulfate and iron reducers (fig. S7 and tables S6 and S7) (*26*). The presence of *dsrB* but not *mcrA* in these samples suggests that sulfate reducers or other groups, but not methanogens, produce this low $\delta^{13}C$-TOC.

$\delta^{13}C$-TOC at the top (2R) and in the intermediate depth interval (–28.4 to –21.6‰) are close to $\delta^{13}C$-DOC from borehole 1026B (–26.1‰) (Fig. 3B) (*6*). The ^{13}C depletion relative to carbonate is lower than in the other layers (~–20 to –26‰), but also falls in the range of the reductive acetyl CoA pathway (table S7), and, consistent with *mcrA* detection, could be affected by autotrophic methanogenesis. In addition, elevated heterotrophic activity is possible, because degradation of chemoautotrophy-derived OC—for example, by AOM, methanogenesis, or fermentation—would lower the $\delta^{13}C$-carbonate and potentially raise the $\delta^{13}C$-TOC. In fact, the lowest $\delta^{13}C$-carbonate values (to –5.1‰) were measured in the intermediate depth interval (18R) (Fig. 3 and table S5), consistent with a locally conspicuous input of IC from the degradation of chemoautotrophy-derived OC. The alternative explanation, enhanced breakdown of photosynthesis-derived OC in the intermediate depth interval, is unlikely given that sediment inclusions are absent (*9*). Similarly, influx of labile DOC or unaltered DIC from seawater is incompatible with the 7 to 11 thousand year greater DOC age compared with bottom seawater and the 4 to 8‰ decrease in $\delta^{13}C$-DIC along the flowpath from Grizzly Bare outcrop to 1026B and BBS, respectively (*6*, *10*).

To rule out a fossil origin of functional genes and the chemical and isotopic signatures, we incubated pieces from the interior of three rock samples used for functional gene analyses (1R-1-79, 14R-1-11, and 23R-2-21) at 65°C in anoxic, sulfate-rich media containing H_2, acetate, methanol, and dimethyl sulfide as energy substrates (table S8). After 2 years, aliquots were transferred to fresh media and incubated for another 5 years using triple-autoclaved basalt pieces as substrata. By then, low concentrations of ^{13}C-depleted methane (–54 to –65‰) had formed, indicating the presence of active methanogenic microorganisms (table S9).

The variability in $\delta^{34}S$-pyrite, $\delta^{13}C$-TOC, and $\delta^{13}C$-carbonate indicates that micro- and macroscale geochemical changes related to mineralogy, fracturing, and/or fluid flow strongly influence microbial activity. These chemical microniches may explain the coexistence of sulfate reducers and methanogens at U1301 and in other igneous habitats, despite higher energy yields of sulfate reduction compared with methanogenesis (*27*). In addition, some methanogens can survive in the presence of sulfate reducers by consuming noncompetitive methylated substrates (*28*). Because methanogenic substrate usage follows *mcrA* phylogeny (*28*), this explanation is consistent with the ability of a close relative of JdFMG to use methanol (*16*); it is also consistent with the production of biogenic methane in basalt incubations containing sulfate and methanol (table S9 and fig. S8).

Inorganic electron donors used by sulfate reducers and methanogens—e.g., H_2—are likely to derive from serpentinization reactions, whereby Fe(II) minerals—e.g., olivine [$(Mg, Fe)_2SiO_4$], which is abundant in several basalt horizons at U1301 (*9*) (fig. S9 and tables S10 and S11)—are oxidized in abiotic reactions with seawater-derived fluids (*1*). Organic electron donors (for example, short-chain fatty acids and alcohols) are probably produced by breakdown of autochthonous OC (*6*, *27*, *29*) or Fischer-Tropsch–type synthesis (*30*) (table S10). Targeted investigations of potential carbon and energy sources will provide further insights to micro- and macroscale heterogeneity of microbial C and S cycling and thus contribute to a better understanding of chemoautotrophic ecosystems within Earth's oceanic crust.

References and Notes

1. W. Bach, K. J. Edwards, *Geochim. Cosmochim. Acta* **67**, 3871 (2003).
2. K. J. Edwards, T. M. McCollom, H. Konishi, P. R. Buseck, *Geochim. Cosmochim. Acta* **67**, 2843 (2003).
3. C. M. Santelli *et al.*, *Nature* **453**, 653 (2008).
4. M. R. Fisk, S. J. Giovannoni, I. H. Thorseth, *Science* **281**, 978 (1998).
5. O. Rouxel, S. Ono, J. Alt, D. Rumble, J. Ludden, *Earth Planet. Sci. Lett.* **268**, 110 (2008).
6. M. D. McCarthy *et al.*, *Nat. Geosci.* **4**, 32 (2011).
7. J. P. Cowen *et al.*, *Science* **299**, 120 (2003).
8. B. N. Orcutt *et al.*, *ISME J.* **5**, 692 (2011).
9. A. T. Fisher, T. Urabe, A. Klaus, Expedition 301 Scientists, *Proc. IODP 301* (2005).
10. B. D. Walker, M. D. McCarthy, A. T. Fisher, T. P. Guilderson, *Mar. Chem.* **108**, 123 (2008).
11. C. G. Wheat *et al.*, *Geochem. Geophys. Geosyst.* **11**, Q07011 (2010).
12. A. Schippers, B. B. Jørgensen, *Geochim. Cosmochim. Acta* **66**, 85 (2002).
13. M. W. Friedrich, *Methods Enzymol.* **397**, 428 (2005).
14. M. Wagner, A. J. Roger, J. L. Flax, G. A. Brusseau, D. A. Stahl, *Appl. Environ. Microbiol.* **75**, 7086 (1998).
15. T. Lueders, K.-J. Chin, R. Conrad, M. Friedrich, *Environ. Microbiol.* **3**, 194 (2001).
16. G. Zhang *et al.*, *Environ. Microbiol.* **10**, 1850 (2008).
17. F. Wang *et al.*, *Proc. Natl. Acad. Sci. U.S.A.* **106**, 4840 (2009).
18. O. U. Mason *et al.*, *ISME J.* **3**, 231 (2009).
19. K. Knittel, A. Boetius, *Annu. Rev. Microbiol.* **63**, 311 (2009).
20. A. Dhillon, A. Teske, J. Dillon, D. A. Stahl, M. L. Sogin, *Appl. Environ. Microbiol.* **69**, 2765 (2003).
21. G. Webster *et al.*, *FEMS Microbiol. Ecol.* **58**, 65 (2006).
22. S. Ono, N. S. Keller, O. Rouxel, J. C. Alt, *Geochim. Cosmochim. Acta* **87**, 323 (2012).
23. M. D. Rudnicki, H. Elderfield, B. Spiro, *Geochim. Cosmochim. Acta* **65**, 777 (2001).
24. M. S. Sim, T. Bosak, S. Ono, *Science* **333**, 74 (2011).
25. D. E. Canfield, B. Thamdrup, *Science* **266**, 1973 (1994).
26. A. L. Zerkle, C. H. House, S. L. Brantley, *Am. J. Sci.* **305**, 467 (2005).
27. H.-T. Lin, J. P. Cowen, E. J. Olson, J. P. Amend, M. D. Lilley, *Geochim. Cosmochim. Acta* **85**, 213 (2012).
28. W. B. Whitman, T. L. Bowen, D. R. Boone, *The Prokaryotes* **3**, 165 (2006).
29. M. A. Lever *et al.*, *Geomicrobiol. J.* **27**, 183 (2010).
30. T. M. McCollom, J. S. Seewald, *Chem. Rev.* **107**, 382 (2007).

Acknowledgments: We thank B. Jørgensen, M. Sogin, and the IODP Expedition 301 Scientists for advice and support in this project. Funding was obtained from a Schlanger Ocean Drilling Fellowship, a University of North Carolina Dissertation Completion Fellowship, a Marie-Curie Intra-European Fellowship (255135) (all to M.A.L.); the Danish National Research Foundation and the Max Planck Society (both to B. Jørgensen); Europole Mer (to O.R.); the European Research Council Advanced Grant DARCLIFE (to K.-U.H.); the NASA Astrobiology Institute Subsurface Biospheres (to A.T.); the Japan Society for the Promotion of Science (JSPS) Funding Program for Next Generation World-Leading Researchers (NEXT Program) (to F.I.); and the National Science Foundation (NSF-OCE 0622949 and OCE 1129631 to J.C.A.; OCE-0753126 to S.O. and O.R.; and NSF-ODP 0727175 and NSF-STC for Dark Energy Biosphere Investigations to A.T.). We thank three anonymous reviewers for very helpful comments. The geochemical data are available in the supplementary tables. Any use of trade, firm, or product names is for descriptive purposes only and does not imply endorsement by the U.S. government. The functional gene sequence data are available from the GenBank database (accession numbers GU182109 to GU182110 and JX465656 to JX465658).

Supplementary Materials

www.sciencemag.org/cgi/content/full/339/6125/1305/DC1
Materials and Methods
Figs. S1 to S9
Tables S1 to S13
References (*31*–*46*)

23 August 2012; accepted 12 December 2012
10.1126/science.1229240